Probing Interactions Between Ultracold Fermions

G. K. Campbell,[1] M. M. Boyd,[1] J. W. Thomsen,[1] M. J. Martin,[1] S. Blatt,[1] M. D. Swallows,[1] T. L. Nicholson,[1] T. Fortier,[2] C. W. Oates,[2] S. A. Diddams,[2] N. D. Lemke,[2] P. Naidon,[3]* P. Julienne,[3] Jun Ye,[1]† A. D. Ludlow[1]‡

At ultracold temperatures, the Pauli exclusion principle suppresses collisions between identical fermions. This has motivated the development of atomic clocks with fermionic isotopes. However, by probing an optical clock transition with thousands of lattice-confined, ultracold fermionic strontium atoms, we observed density-dependent collisional frequency shifts. These collision effects were measured systematically and are supported by a theoretical description attributing them to inhomogeneities in the probe excitation process that render the atoms distinguishable. This work also yields insights for zeroing the clock density shift.

Quantum statistics plays a critical role in shaping interactions between matter. This is apparent in the markedly different behavior of Bose-Einstein condensates (1, 2) and degenerate Fermi gases of ultracold atoms (3). The quantum statistics of atoms can thus be a key factor in the choice of an atomic system for a given experiment. Such is the case for atoms at the heart of an atomic clock. Simultaneous interrogation of many atoms is favorable for achieving high measurement precision. However, when atoms interact with each other, their internal energy states can be perturbed, leading to frequency shifts of the clock transition (4, 5). The use of identical fermions was prescribed to allow many atoms to strengthen the signal without such density-dependent collision shifts (6). Previous experiments seemed to confirm this fact for both single-component (7) and two-component fermion mixtures (8).

However, by probing an optical clock transition with thousands of fermionic Sr atoms confined in a one-dimensional optical lattice, we clearly observe density-related frequency shifts at a fractional precision of 1×10^{-16}. When the light-atom interaction introduces a small degree of inhomogeneous excitation, previously indistinguishable fermions become slightly distinguishable. This effect causes a time-dependent variation of the two-particle correlation function,

giving rise to an apparent mean-field energy. The resulting collision effects have been measured systematically as a function of temperature, excitation probability, and interaction inhomogeneity. These observations are supported by a theoretical description of fermionic interactions that includes the effect of the measurement process.

The latest generation of optical atomic clocks such as those based on the $^1S_0$–$^3P_0$ transition in fermionic ^{87}Sr currently offers the highest measurement precision, useful for measuring possible atomic interactions (9, 10). In an ultracold dilute gas with a mean-field energy, a narrow clock transition will experience a density-dependent frequency shift (11, 12) given by $h\Delta\nu = (4\pi\hbar^2 G^{(2)}\rho a)/m$. Here, m is the atomic mass, ρ is the density of the atomic sample, a is the s-wave scattering length characterizing the atomic interaction, and $h = 2\pi\hbar$ is Planck's constant. $G^{(2)}$ is the two-atom correlation function at zero distance, which summarizes the quantum statistics of colliding bodies. For example, $G^{(2)} = 0$ for identical fermions and $G^{(2)} = 2$ for identical bosons in a thermal gas. The Fermi suppression arises from the Pauli exclusion principle, which prohibits even-partial-wave collisions between indistinguishable fermions. At ultracold temperatures, partial waves higher than s-wave are frozen out (13). For atoms excited in our two-level clock system, three possible s-wave interactions exist: those between two $^1S_0$ ground-state ($|g\rangle$) atoms, those between two $^3P_0$ excited-state ($|e\rangle$) atoms, and those between a $|g\rangle$ atom and a $|e\rangle$ atom. Including all possible in-

[1]JILA, National Institute of Standards and Technology and University of Colorado Department of Physics, University of Colorado, Boulder, CO 80309–0440, USA. [2]Time and Frequency Division, National Institute of Standards and Technology, Boulder, CO 80302, USA. [3]Atomic Physics Division and Joint Quantum Institute, National Institute of Standards and Technology, 100 Bureau Drive Stop 8423, Gaithersburg, MD 20899–8423, USA.

*Present address: ERATO (Exploratory Research for Advanced Technology) Macroscopic Quantum Project, Japan Science and Technology Agency, Tokyo, 113-0033, Japan.
†To whom correspondence should be addressed. E-mail: junye@jilau1.colorado.edu
‡Present address: Time and Frequency Division, National Institute of Standards and Technology, Boulder, CO 80302, USA.

Fig. 1. (**A**) Sideband excitation spectra for $T = 1$ μK (blue circles) and 3 μK (red squares). The spectra are obtained in the resolved sideband limit and have three dominant features, the narrow carrier transition and broad red (blue) motional sidebands that are excited when an atom is transferred to a lower (higher) motional state during the transition. As the temperature of the sample is lowered, the atoms primarily occupy the ground state and the red sideband is suppressed. The temperature of the atomic ensemble can be extracted from a fit of the sidebands (25). The inset shows the lattice geometry and excitation scheme. The probe beam and lattice are co-aligned and copolarized, minimizing the relative spread between $\vec{k}_l$ and $\vec{k}_p$. However, even with the best effort, a small angle $\Delta\theta$ between the probe and lattice beams may persist due to aberrations and misalignment. (**B**) Rabi oscillations for temperatures of 1 μK (blue circles) and 3 μK (red squares). For higher temperatures, more motional states are occupied. This leads to a larger spread in the Rabi frequencies and faster dephasing of the excitation between atoms. By fitting the decay of Rabi oscillations, we can determine the degree of excitation inhomogeneity. The inset illustrates the dephasing process with rotations on the Bloch sphere. At time a, before the excitation, the atoms are in a pure state. At time b, the atoms have undergone two oscillations. For the red curve, the temperature is hotter and there is a larger spread in Rabi frequencies. This is indicated by the increased width of the Bloch vector and dephasing of the observed oscillations. At time c, the effect is even more pronounced.
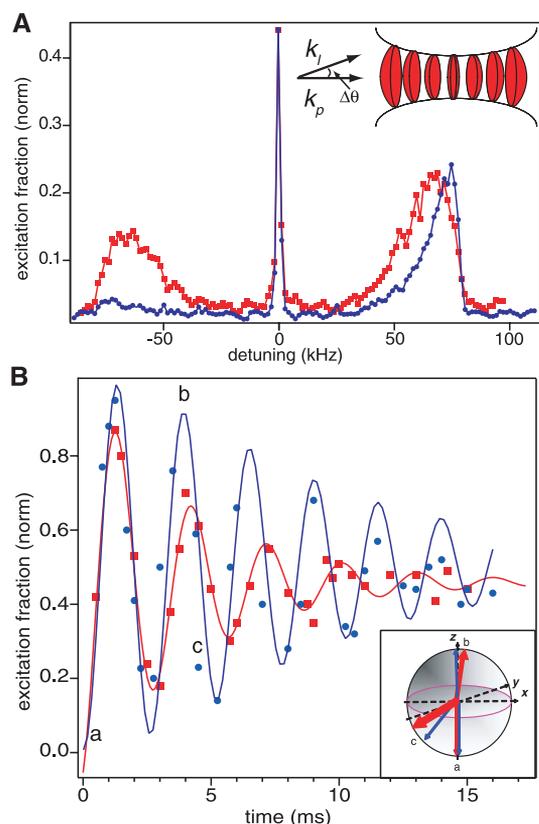
teractions, the collisional frequency shift at ultra-cold temperatures is given by Eq. 1 (8, 12, 11):

$$\Delta\nu_{ge} = \frac{2\hbar}{m}(G_{ge}^{(2)}a_{ge}(\rho_g - \rho_e) +$$

$$G_{ee}^{(2)}a_{ee}\rho_e - G_{gg}^{(2)}a_{gg}\rho_g) \quad (1)$$

where a_{ij} is the s-wave scattering length for collisions between atoms in state i and j, and ρ_i is the density of atoms in state i. Because indistinguishable fermions do not collide, $G_{gg}^{(2)} = G_{ee}^{(2)} = 0$. Fermions in different internal states are distinguishable, and for a completely incoherent mixture of the two states, $G_{ge}^{(2)} = 1$. However, if the two-state mixture is prepared by a uniform, coherent excitation of ground-state atoms, then the fermions evolve indistinguishably and $G_{ge}^{(2)} = 0$ (8). In this case, $\Delta\nu_{ge} = 0$.

Two possibilities exist for $\Delta\nu_{ge}$ to deviate from zero. First, the p-wave contribution may not be negligible. However, for ultracold atoms confined in a well-characterized optical trap, we show experimental evidence and theoretical calculations that conclude that p-wave collisions make no noticeable contribution to the observed clock frequency shift. Second, it is imperative to consider the entire interaction, including the measurement process, when exploring the question of whether fermions collide. Indeed, the measurement process, such as probing a clock transition, may strongly influence the value of $G^{(2)}$. We show here that an inhomogeneous interaction between light and atoms leads to the loss of indistinguishability of the fermions, thus making $0 < G^{(2)} < 1$.

Although a uniform, coherent excitation of identical fermions maintains $G^{(2)} = 0$, and no s-wave collisions occur, if a small nonuniformity in the excitation process arises, the atoms are no longer completely identical, and $G^{(2)} > 0$. The value of $G^{(2)}$ will depend on the degree of excitation inhomogeneity. This measurement-induced dynamic variation of quantum statistics leads directly to a change of the mean-field energy within the ultracold gas, resulting in a nonzero $\Delta\nu_{ge}$. It is interesting to contrast the present work with previous results observed with an ultracold gas of fermionic ^{6}Li, where the insensitivity of a radio-frequency (rf) transition to collisional shifts was demonstrated (7, 8). It was shown that the fermionic insensitivity to collisional shifts was maintained even when a pure superposition state of the two-level system had decohered. This decoherence does allow interactions, but when a uniform rf probing field reintroduced coherence to the atoms in a homogeneous manner, the apparent value for $G^{(2)}$ again became zero, giving no collisional shifts within the measurement precision (14). From the current experiment, it is clear that any nonidentical evolutions during the interrogation process lead to the breakdown of Fermi suppression; this experiment is sensitive to very small inhomogeneities because of the high measurement precision.

An intuitive understanding emerges from considering two sample atoms in a pseudo spin-1/2 system with ground $|g\rangle$ and excited $|e\rangle$ states. Before applying the spectroscopy pulse, the atomic system is in a pure, polarized spin state with $|\psi_1\rangle = |\psi_2\rangle = |g\rangle$. The effect of the pulse is to perform a rotation on the Bloch sphere, as shown in the inset of Fig. 1B. For a coherent, homogeneous excitation, the wave function of the system becomes a coherent superposition $|\psi_1\rangle = |\psi_2\rangle = \alpha|g\rangle + \beta|e\rangle$. The wave functions of both atoms are identical, $G_{12}^{(2)} = 0$, and collisions cannot occur. An inhomogeneous spectroscopic excitation, such as that caused by varying Rabi frequencies for different atoms, results in slightly different rotations on the Bloch sphere for the two atoms (Fig. 1B, inset). Hence, we have $|\psi_1\rangle = \alpha|g\rangle + \beta|e\rangle$ and $|\psi_2\rangle = \gamma|g\rangle + \delta|e\rangle$. The fermions are distinguishable and $0 < G_{12}^{(2)} \leq 1$. The value of $G_{12}^{(2)}$ depends on the amount of inhomogeneity, and its time variation can be explicitly calculated from the antisymmetrized overlap of the two wave functions [details are provided in the supporting text (15)]:

$$G_{12}^{(2)}(\alpha(t),\beta(t),\gamma(t),\delta(t)) =$$
$$1 - |\alpha(t)\gamma^*(t) + \beta(t)\delta^*(t)|^2 \quad (2)$$

The resulting collision shift from Eq. 1 is then

$$\Delta\nu(t) = \frac{2\hbar a_{ge}}{m}G_{12}^{(2)}(\alpha,\beta,\gamma,\delta)(\rho_g - \rho_e) \quad (3)$$

Before proceeding with experimental results, we first summarize the system under study (15). In the ^{87}Sr optical clock, atoms are trapped in a one-dimensional (1D) optical standing-wave potential (1D optical lattice). Longitudinally the atoms are confined tightly, with an oscillation frequency $\nu_z \sim 80$ kHz. At temperature $T = 1$ μK, ~ 98% of the atoms occupy the ground state of the trap ($\bar{n}_z = 0.02$). The laser probing the clock transition propagates along the lattice axis, and spectroscopy is performed in the Lamb-Dicke regime. In the transverse plane the confinement is much weaker, with an oscillation frequency $\nu_x = \nu_y \sim 450$ Hz, and atoms occupy a large number of motional states $\bar{n}_x = \bar{n}_y = 46$). Typically, ~2 × 10^3 atoms are trapped in the optical lattice, resulting in 30 atoms per lattice site with a density of 2×10^{11} cm^{-3} (15). The optical lattice is nearly vertically oriented and is operated at the so-called magic wavelength of $\lambda_L \sim 813.429$ nm (16), where the ac Stark shifts of the $^1S_0$ and $^3P_0$ states are identical.

With a perfect alignment of the probe laser along the strong confinement axis, assuming cylindrical symmetry, a residual angular spread between the probe and lattice $\vec{k}$ remains due to the finite size of the lattice beam (17). However, an even larger effect occurs if the symmetry is broken due to either aberrations in the beam profile or angular misalignment ($\Delta\theta$) between the lattice and the probe beam. For our trap parameters, we estimate an effective $\Delta\theta \approx 10$ mrad (Fig. 1A, inset). The residual wave vector projected on the transverse plane leads to slightly different excitation Rabi frequencies $\Omega_{\vec{n}}$ for atoms in different (n_x, n_y) states (15, 18, 19). For a given T, the occupation of a transverse motional state $n_{x,y}$ is given by the normalized Maxwell-Boltzmann distribution. The inhomogeneity in the Rabi frequencies is thus affected by both T and $\Delta\theta$.

To calculate the density shift, we return to our two-atom model. Each atom has a slightly different $\Omega_{\vec{n}}$. For the entire atomic ensemble, we can define an average Rabi frequency $\overline{\Omega}$ and its

Fig. 2. Measured density-dependent frequency shift as a function of the final excitation fraction and temperature. Atoms are initially spin polarized and transferred to $^3P_0$ ($|e\rangle$) before the spectroscopy pulse is applied. The squares (circles) show the measured shift for $T = 1$ (3) μK. The lines show the calculated shifts when the two-atom model is used with only a single scaling factor. Near ~50% the shift goes through zero. In the inset, the measured shift is shown for atoms excited from the $^1S_0$ ($|g\rangle$) state for $T = 1$ μK (squares), 3 μK (circles), and 5 μK (triangles). However, the magnitude in this case could be influenced by imperfect spin polarizations. For both plots, as the temperature is decreased, the inhomogeneity also decreases, leading to a smaller collision shift. ρ is the atomic density of 10^{11}/cm^3. The density-dependent shift for each excitation fraction is determined with an interleaved scheme in which the density is varied every 100 s. Pairs of such data are then used to determine the frequency shift. Typical data sets include 20 to 30 pairs of density comparison, with the error bars indicating the standard error (SE).
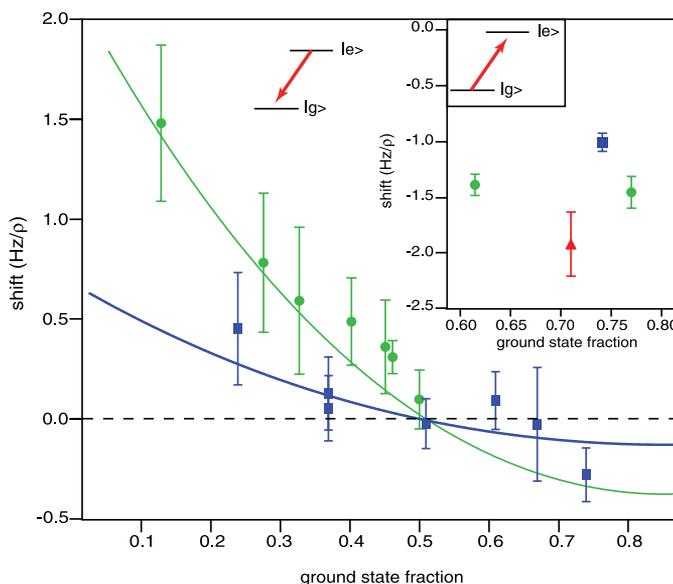
root mean square spread $\Delta\Omega$. To approximate the average density shift, we set $\Omega_1 = \overline{\Omega} + \Delta\Omega$ and $\Omega_2 = \overline{\Omega} - \Delta\Omega$ for our two-atom model. Thus, the time-dependent quantities α, β, γ, and δ as defined in Eq. 2 are parameterized by $\overline{\Omega}$ and $\Delta\Omega$ (15). At a time t during the spectroscopy pulse, the atoms experience an ensemble-averaged shift:

$$\Delta\nu(t) =$$
$$\frac{2\hbar a_{ge}}{m} G_{12}^{(2)}(\overline{\Omega} + \Delta\Omega, \overline{\Omega} - \Delta\Omega)(\rho_g - \rho_e) \quad (4)$$

This shift evolves during the spectroscopy pulse, and for the final density shift we time average $\Delta\nu(t)$ over the total pulse length t_F. This approximation is valid in the limit that the change in Ω due to atomic interactions is much less than $\Delta\Omega$. A more rigorous calculation with the optical Bloch equations that includes atomic interactions has also been made. Using our typical trap parameters, we find that the two-atom approximation is valid to within 5%. The time-dependent Rabi oscillation is only slightly affected by atomic interactions; however, the effect on the final clock shift is obvious.

For inhomogeneity-induced collision shifts, t_F is important. Atoms in close proximity to each other tend to have similar Rabi frequencies, whereas atoms located far apart are more likely to experience different excitations (and hence be distinguishable). If $t_F\nu_{x,y} \ll 1$, the atoms are effectively frozen in place and will experience no density shift. However, if $t_F\nu_{x,y} > 1$, atoms initially located far apart have time to interact. For the clock experiment requiring high spectral resolution, $t_F = 80$ ms and $1/\nu_{x,y} = 2.2$ ms, so collisions will occur.

To systematically study these effects, we implemented controlled variations of both T and $\Delta\theta$. To vary T, we perform cooling (heating) of the lattice-confined atoms in three dimensions: Doppler cooling (heating) along the transverse direction and sideband cooling (heating) along the longitudinal axis. Simultaneous with the sideband cooling (heating), the atoms are spin-polarized by optical pumping in a weak magnetic (B) bias field. Atoms are polarized into either the $m_F = +9/2$ or $m_F = -9/2$ Zeeman states. The $^1S_0$–$^3P_0$ clock transition, which is predicted to have a natural linewidth of ~1 mHz (20–22), is interrogated with a cavity-stabilized diode laser at 698 nm with a linewidth below 1 Hz (23). Spectroscopy is performed in the Lamb-Dicke regime and in the resolved sideband limit (24). To ensure that the polarized spin state is well resolved from other m_F levels, spectroscopy is performed under $B \sim 250$ mG, leading to a separation of 250 Hz between the $m_F = \pm9/2$ states. A spectroscopy pulse length of $t_F = 80$ ms results in a Fourier-limited linewidth of ~10 Hz.

After the spectroscopy pulse is applied, atoms remaining in $|g\rangle$ are counted by measuring fluorescence on the strong $^1S_0$–$^1P_1$ transition. Atoms transferred to $|e\rangle$ are then pumped back to $|g\rangle$ via the intermediate $(5s6s)^3S_1$ states and are also

counted. Combining these two measurements gives us a normalized excitation fraction $\rho_e/(\rho_e + \rho_g)$. The atomic temperature is determined by sideband spectroscopy (25, 15) and time-of-flight analysis. In Fig. 1A, sample spectra are shown for two different values of T. Once T is measured, the degree of inhomogeneity is determined by fitting the decaying Rabi oscillations for the ensemble. In Fig. 1B, the Rabi oscillation at $T = 3$ µK (squares) clearly shows faster dephasing than that of $T = 1$ µK (circles), indicating a larger degree of inhomogeneity.

Density-dependent frequency shifts of the ^{87}Sr clock transition are measured with a remotely located calcium optical standard at the National Institute of Standards and Technology (NIST) (9) as a stable frequency reference, which is linked to JILA via a phase-coherent fiber network (26). This direct optical frequency measurement between two optical standards allows fractional measurement precision of a few times 10^{-16} after hundreds of seconds of averaging. To measure the clock center frequency, the spectroscopy pulse is first applied to atoms optically pumped to the $m_F = +9/2$ state. In the next cycle, atoms polar-

ized to the $m_F = -9/2$ state are used. The center frequency is then determined by the average of both resonances. The density-dependent frequency shift is determined with an interleaved scheme, in which the density of the atomic ensemble is varied every 100 s. The density is varied by a factor of 2. Pairs of such data are then used to measure a frequency shift, and many pairs are averaged to decrease the statistical uncertainty. Typically, we lock the clock laser near the full-width at half-maximum of each resonance; however, the location of the lock points is varied to select the desired excitation fraction.

Spectroscopy is performed by means of two different experimental procedures. In the first, we probe the clock transition from $|g\rangle$ to $|e\rangle$ (Fig. 2, inset). The intensity of the probe is set to produce a π pulse on resonance. This direct scheme could suffer from imperfect polarization of the atomic sample, and spectator atoms could be left in other m_F levels. This scenario could potentially lead to density-dependent shifts due to collisions between different m_F states that are not suppressed by the Fermi statistics. The second scheme minimizes this effect by probing $|e\rangle$ to $|g\rangle$ (Fig. 2).
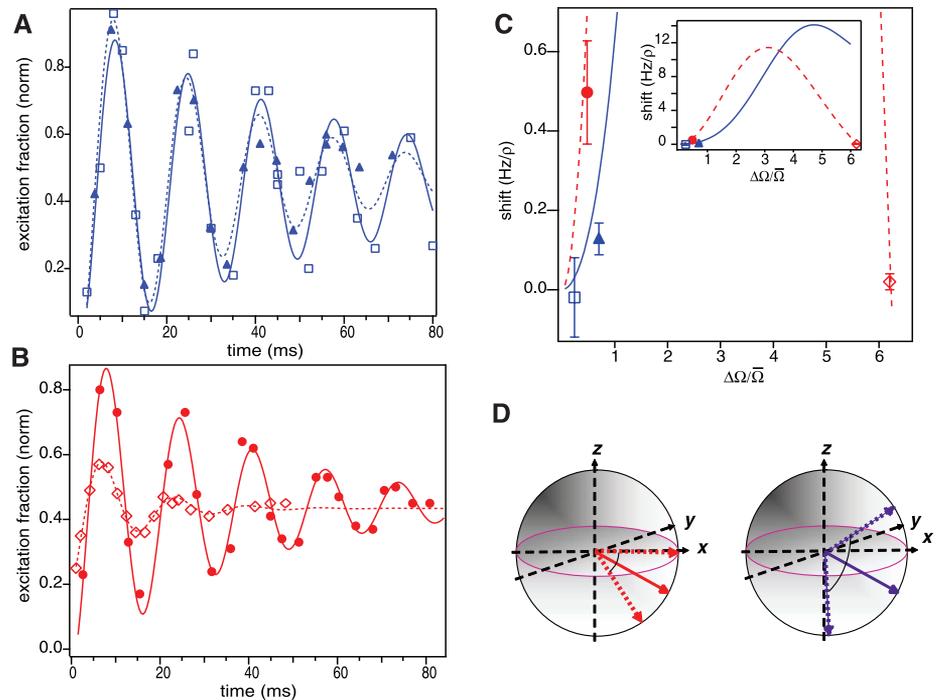

Fig. 3. Effect of probe misalignment on the density-dependent shift. (**A**) Rabi oscillations are shown for two different values of $\Delta\theta$ at $T = 1$ µK. The open squares show oscillations when the probe is aligned similar to that of Figs. 1 and 2. The solid triangles show a faster dephasing when the probe beam misalignment is increased further by 5 mrad. (**B**) Rabi oscillations for $T = 3$ µK. The circles show oscillations when the probe beam is aligned similar to that of Figs. 1 and 2, and the diamonds when the misalignment is increased further by 35 mrad. (**C**) The density shift measured for each misalignment shown in (A) and (B). From $\Delta\theta$ and T, the spread in Rabi frequency $\Delta\Omega$ is calculated. The lines show the expected shift as a function of $\Delta\Omega$ for $T = 1$ µK (solid line) and 3 µK (dashed line). The inset shows a zoomed-out plot. (**D**) For large misalignments, we observe a smaller density shift. This is described with the rotation on the Bloch sphere. As an example, two different values of $\Delta\Omega$ are shown. On each sphere, the average excitation fraction is shown with a solid line, and the spread is indicated by the dotted lines. For small misalignments, we have a small spread in Rabi frequencies. As the misalignment increases, the spread crosses the equatorial plane of the Bloch sphere. At 50%, the sign of the density shift changes, and therefore the portion of the spread centered around this plane averages to zero. The measured density shift is then reduced.

Here, we apply a strong pulse to first transfer the population from $|g\rangle$ to $|e\rangle$. The pulse power broadens the transition in order to decrease the sensitivity of population transfer to probe laser frequency, and transfers ~50% of the population to $|e\rangle$. This first pulse is resonant with atoms in one of the $m_F = \pm 9/2$ states, hence atoms left in other m_F states due to imperfect polarization are not transferred. Subsequently, all atoms remaining in $|g\rangle$ are removed from the lattice with a pulse of light resonant with the strong $^1S_0-^1P_1$ transition, without affecting the temperature of the atoms in $|e\rangle$. This is confirmed with sideband spectroscopy (15). Finally, the clock transition of $|e\rangle$ to $|g\rangle$ is probed with the usual 80-ms π pulse. In both experimental procedures, we measure populations in $|e\rangle$ and $|g\rangle$ to determine the normalized excitation fraction.

Figure 2 summarizes the measured density-dependent frequency shift as a function of the normalized ground-state fraction for two different values of T, 1 μK (squares) and 3 μK (circles). The data indicate a clear trend that the density shift decreases under a more homogeneous excitation. The solid lines are the expected shifts calculated from the two-atom model. For clock operation, it is important to note that near 50% excitation fraction, for both values of T, the shift goes through zero.

As we change T, we vary both the excitation inhomogeneity and the p-wave contribution. To estimate the magnitude of p-wave collisions, we note that the van der Waals potential for all three interaction types (gg, ee, or eg) has been theoretically calculated (27, 21, 28), and the p-wave centrifugal barrier is expected to be greater than 25 μK. At $T \sim 1$ μK, $ka \ll 1$, where $k = 2\pi/\lambda_T$. $\lambda_T = h/\sqrt{2\pi m k_B T}$ is the thermal de Broglie wavelength, and k_B is the Boltzmann constant. Under these conditions, the ratio of p-wave to s-wave phase shift is $(bk)^2 b/a$, where b is the p-wave scattering length. For gg interactions, the s-wave scattering length has been measured (29) for ^{88}Sr, and mass scaling gives $a_{gg} = 96.2(1)a_0$ for ^{87}Sr, where a_0 is the Bohr radius. Combined with the van der Waals potential, the p-wave phase shift can be determined from the Schrödinger equation. For $^1S_0$, $b_{gg} = -76 \, a_0$, and for $T = 1$ μK, $|(b_{gg}k)^2 b_{gg}/a_{gg}| \approx 0.01$. Thus, p-wave collisions for gg are suppressed by more than two orders of magnitude and are negligibly small. Although the s-wave scattering lengths a_{ee} and a_{ge} have not yet been measured and thus cannot directly constrain the values of b_{ee} and b_{eg}, calculations based on a theoretical potential predict that these p-wave collisions are similarly suppressed relative to s-wave collisions. An exception would be a p-wave shape resonance (13); however, this would occur only for a very small range of possible a_{ee} and a_{ge}, and the effect would be reduced by thermal averaging. We also note that in a trapping potential, k is modified due to the zero-point energy of the trap (k_{ZP}) and the effective thermal wave vector for collisions is given by $k_T = \sqrt{(k^2 + k_{ZP}^2)/2}$. For our trap,

$k_{ZP} \sim 3.5$ μK, and p-wave collisions are still suppressed. The observed density shift scales as $G_{12}^{(2)} a_{ge}$, and for our typical temperatures we find values of $G_{12}^{(2)}$ between 0.03 and 0.15, whereas the p-wave scattering length is expected to be ~1% of a_{ge}. Hence, inhomogeneity-induced s-wave collisions dominate. In the unitarity limit where $k_T|a_{ge}| > 1$ (a_{ge} is the zero-temperature scattering length), the effective scattering length is $1/k_T$. For our lattice trap parameters and temperature range of 1 to 3 μK, this length is on the order of $-300 \, a_0$, which is consistent in sign and magnitude with our observed frequency shifts, along with the values and uncertainties of $G_{12}^{(2)}$ and ρ.

To provide further evidence to exclude p-wave contributions, we vary the inhomogeneity by misalignment of the spectroscopy probe beam under a fixed T. This also helps rule out $\bar{n}_{x,y,z}$-dependent residual ac Stark shift of the trap. Typically the probe beam is coaligned with the lattice to minimize motional effects. However, by increasing the misalignment ($\Delta\theta$), we can also increase $\Delta\Omega$. Figure 3, A and B, show Rabi oscillations for two different probe beam misalignments at $T = 1$ μK (triangles and open squares) and 3 μK (circles and open diamonds), respectively. Figure 3C displays the measured density shift as a function of ($\Delta\Omega/\overline{\Omega}$) due to probe misalignment. For $T = 1$ μK, the shift becomes larger with increased $\Delta\Omega/\overline{\Omega}$. When $\Delta\Omega/\overline{\Omega}$ increases further, the 3 μK data indicate that the density shift becomes smaller. This behavior is reproduced by the theoretical curves shown in Fig. 3C and is illustrated in Fig. 3D. Consider two different $\Delta\Omega/\overline{\Omega}$, both with an average excitation fraction of 0.3. In the first case, for small misalignment, we find a spread in the excitation fraction of ±0.2; there is an inhomogeneity allowing collisions to occur, and we measure a small density shift. In the second case, with further misalignment the spread in the excitation fraction increases to ±0.4; there is now a larger spread in the Rabi frequencies, and collisions still occur. However, we now have atoms with an excitation fraction both above and below 50% where the shift crosses zero. Hence, the collisions of atoms with excitations between 0.3 and 0.7 will average to zero (this is consistent with the density shift going to zero at 50% excitation, regardless of the inhomogeneity), and the final collision shift is due only to atoms with excitation fractions between 0 and 0.3. The measured shift for the larger misalignment is therefore smaller.

Combining the measurements shown in Figs. 2 and 3 makes it clear that the observed density-dependent shifts arise from the change of the quantum statistics $G^{(2)}$ caused by the inhomogeneous measurement process. The inhomogeneous effect can be suppressed by decreasing the sample temperature and increasing the transverse confinement, or going to higher dimension traps. For clock operations, we have shown that near a 50% excitation fraction, the density shift goes to zero. Using these measurements, we can now reduce the uncertainty of the collision shifts for clock

operation (9) to 5×10^{-17}. This time-dependent variation in quantum statistics will also apply to boson-based clocks, where the original $G^{(2)} = 2$ will decrease to a value between 1 and 2.

References and Notes

1. E. A. Cornell, C. E. Wieman, *Rev. Mod. Phys.* **74**, 875 (2002).
2. W. Ketterle, *Rev. Mod. Phys.* **74**, 1131 (2002).
3. B. DeMarco, D. S. Jin, *Science* **285**, 1703 (1999).
4. K. Gibble, S. Chu, *Phys. Rev. Lett.* **70**, 1771 (1993).
5. Y. Sortais et al., *Phys. Scr.* **T95**, 50 (2001).
6. K. Gibble, B. J. Verhaar, *Phys. Rev. A* **52**, 3370 (1995).
7. S. Gupta et al., *Science* **300**, 1723 (2003).
8. M. W. Zwierlein, Z. Hadzibabic, S. Gupta, W. Ketterle, *Phys. Rev. Lett.* **91**, 250404 (2003).
9. A. D. Ludlow et al., *Science* **319**, 1805 (2008).
10. G. K. Campbell et al., *Metrologia* **45**, 539 (2008).
11. P. J. Leo, P. S. Julienne, F. H. Mies, C. J. Williams, *Phys. Rev. Lett.* **86**, 3743 (2001).
12. D. M. Harber, H. J. Lewandowski, J. M. McGuirk, E. A. Cornell, *Phys. Rev. A* **66**, 053616 (2002).
13. B. DeMarco, J. L. Bohn, J. P. Burke, M. Holland, D. S. Jin, *Phys. Rev. Lett.* **82**, 4208 (1999).
14. In the experiments of (8), an rf transition was measured, where the effect due to inhomogeneous excitations and the motion of atoms was far below their measurement precision.
15. Materials and methods are detailed in the supporting material available on *Science* Online.
16. J. Ye, H. J. Kimble, H. Katori, *Science* **320**, 1734 (2008).
17. P. J. Martin, B. G. Oldaker, A. H. Miklich, D. E. Pritchard, *Phys. Rev. Lett.* **60**, 515 (1988).
18. D. J. Wineland, W. M. Itano, *Phys. Rev. A* **20**, 1521 (1979).
19. T. Akatsuka, M. Takamoto, H. Katori, *Nat. Phys.* **4**, 954 (2008).
20. M. M. Boyd et al., *Phys. Rev. A* **76**, 022510 (2007).
21. R. Santra, K. V. Christ, C. H. Greene, *Phys. Rev. A* **69**, 042510 (2004).
22. S. G. Porsev, A. Derevianko, *Phys. Rev. A* **69**, 042506 (2004).
23. A. D. Ludlow et al., *Opt. Lett.* **32**, 641 (2007).
24. D. Leibfried, R. Blatt, C. Monroe, D. Wineland, *Rev. Mod. Phys.* **75**, 281 (2003).
25. By analyzing the spectral components in sideband spectroscopy, the longitudinal temperature can be accurately determined. Extracting the transverse temperature is more complicated; however, using time-of-flight analysis, we have confirmed that the transverse and longitudinal temperatures are identical both before and after cooling (heating).
26. S. M. Foreman et al., *Phys. Rev. Lett.* **99**, 153601 (2007).
27. S. G. Porsev, A. Derevianko, *Phys. Rev. A* **65**, 020701 (2002).
28. We have calculated the phase shifts, and corresponding lengths, using a model S+P potential with variable short-range shapes to change the scattering length over its full range. The short-range shape parameter varies so as to change the threshold phase and scattering length, corresponding approximately to changing the number of bound states in the potential by one. This represents the possible ranges of variation of any Sr van der Waals potential.
29. Y. N. M. de Escobar et al., http://arxiv.org/abs/0808.3434v1 (2008).
30. We appreciate technical contributions of T. Zelevinsky and insightful discussions with K. Gibble, W. Ketterle, M. Zwierlein, E. Cornell, and S. Kokkelmans. We acknowledge funding support from NIST, NSF, Office of Naval Research, and Defense Advanced Projects Research Agency. G.K.C. and A.D.L. are supported by National Research Council postdoctoral fellowships. J.W.T. is a JILA visiting fellow, with a permanent address: The Niels Bohr Institute, Universitetsparken 5, 2100 Copenhagen, Denmark.